Influence of Physical Characteristics of Ceria Particles on Polishing Rate of Chemical Mechanical Planarization for Shallow Trench Isolation

Japanese Journal of Applied Physics
Vol. 43, No. 11A, 2004, pp. 7427–7433

Influence of Physical Characteristics of Ceria Particles on Polishing Rate of Chemical Mechanical Planarization for Shallow Trench Isolation

Sang-Kyun KIM, Phil-Won YOON, Ungyu PAIK*, Takeo KATOH[1] and Jea-Gun PARK[1]

Department of Ceramic Engineering, Hanyang University, 17 Haengdang-Dong, Seoungdong-Gu, Seoul 133-791, Korea
[1]*Nano-SOI Process Laboratory, Hanyang University, 17 Haengdang-Dong, Seoungdong-Gu, Seoul 133-791, Korea*

(Received April 9, 2004; accepted July 7, 2004; published November 10, 2004)

By considering the physical characteristics of ceria particles, the factors affecting the chemical mechanical planarization (CMP) performance for shallow trench isolation (STI) were investigated. Ceria powders were synthesized by calcination at temperatures of 400, 600, 700, 800, and 900°C. The influence of the calcination temperature on the physical characteristics, such as the crystallinity, grain size, porosity, morphology and high-resolution lattice images of the ceria particles, were investigated, and a correlation between the physical characteristics and the electrokinetic behaviors of the ceria particles in aqueous suspending media was also investigated to identify the relationship with CMP performance. Grain size increased with calcination temperature, as did the removal rate of plasma-enhanced tetraethylorthosilicate (PETEOS) film with slurries including these particles. The results indicate that the grain size of ceria particles is one of the key parameters controlling the removal rate and uniformity of PETEOS film. [DOI: 10.1143/JJAP.43.7427]

KEYWORDS: chemical mechanical planarization, CMP, shallow trench isolation, STI, ceria, grain size

1. Introduction

The shallow trench isolation (STI) method has replaced the local oxidation of silicon (LOCOS) method because of its excellent ability to decrease isolation width, leading to improved device density.[1)] Chemical mechanical polishing (CMP) is applied as a key process in the STI method. Compared with other abrasive materials used in polishing slurry for STI CMP, cerium oxide or ceria (CeO_2) is commonly used in ultra-large-scale integration (ULSI) processes because it provides high removal rates, due to its chemical reactivity with silica substrates, and a high removal selectivity between oxide and nitride films.[2,3)] The reaction between cerium oxide and glass/SiO_2 film results in the formation of a chemical "tooth" between the silica surface and the ceria particles, inducing a localized strain in the glass with particle movement.[4)] Consequently, the Si–O–Ce bonds can be rapidly removed by the mechanical force generated by the pressed pad and the abrasive particles, and physical properties, such as good crystallinity, lead to a high removal rate for glass/SiO_2 film.

The physical properties of ceria particles in slurry can significantly affect the oxide film removal rate and the presence of CMP-induced defects, such as micro-scratches or dishing, in the STI CMP process.[5,6)] Recently, researchers[7–9)] have shown interest in the physical aspects as well as the chemical aspects, of the CMP mechanism. The physical properties of ceria particles, such as the crystallinity, particle roughness, and morphology, depend on the synthesis method.[9)] Several methods of preparing cerium oxide have been reported in the literature: the solid-state displacement technique,[10,11)] wet precipitation,[12)] sol–gel technology,[13)] the hydrothermal technique,[14)] electrochemical synthesis,[15)] the inert gas condensation technique,[16)] mechanochemical synthesis,[17)] and the flux method.[18)] The key parameter of the physical properties affecting STI CMP performance, however, has not specifically been addressed yet. Additionally, the physical properties of the ceria particles affect the electrokinetic behavior of CeO_2 particles in an aqueous medium. The electrokinetic behavior of the abrasive particles is an essential factor in the improved performance of the slurry, since it is influenced by differences in the surface potentials of ceria abrasives and oxide plasma-enhanced tetraethylorthosilicate (PETEOS) and CVD Si_3N_4 films.[2)]

In this study, ceria particles were prepared by the solid-state decomposition method, as the particles synthesized by this technique have a higher removal rate for glass/SiO_2 film than any of the other synthesis methods.[9)] Additionally, with this process it is simpler and more convenient to control the physical properties of ceria. We investigated the physical properties of ceria particles by controlling the calcination temperature in the solid-state decomposition method and examining the resulting CMP performance, including the PETEOS removal rate in the STI CMP process. We have attempted to correlate the physical properties of ceria particles, as controlled by the calcination temperature, with the CMP performance.

2. Experimental

Ceria powders were synthesized by the solid-state decomposition method in this study. This method employs high-purity cerium carbonate [$Ce(CO_3)_3$, reagent grade, United International, Inc., Germany] as a starting material. The ceria powders were synthesized by calcination under an air atmosphere at various temperatures (400, 600, 700, 800, and 900°C) for 4 h, resulting in the formation of ceria powder. The mechanical milling of ceria powder was carried out with a basket-type Mixer/Mill (Ring Mill, Dae Yang, Inc., Korea) using zirconia balls (0.8 mm diameter).

The prepared powders were then characterized by various methods. The decomposition behavior of the calcined precursor was monitored by simultaneous (TG and DTA) thermal analyses (SDT 2960, TA Instruments) up to 900°C at a heating rate of 10°C/min in synthetic air (~20%, O_2), and using alumina (Alumalox, Alcoa) as a reference material. The crystal structure was analyzed with a diffractometer (RINT/DMAX-2500, Rigaku, Japan) using Cu-Kα radiation ($\lambda = 0.1542$ nm) at a scan rate of $2^\circ\,\mathrm{min}^{-1}$ ($2\theta\,\mathrm{min}^{-1}$). The intensity was logged over a 2θ range of

*E-mail address: upaik@hanyang.ac.kr

25–60° with a scan step of 0.02°. The grain sizes of the calcined powders were estimated using an X-ray line broadening method, by applying the Debye–Scherrer equation.[19] The powder morphology was observed by transmission electron microscopy (TEM; JEM-2010, JEOL, Japan) at an acceleration voltage of 200 kV.

After analyzing the prepared powders, they were dispersed in deionized water. Drops of the resulting suspensions were put on a microscopic grid previously covered with a polymer and carbon film. Nitrogen adsorption/desorption on the powder surface (Micromeritics, ASAP 2010) was used to measure specific surface area (m^2/g) and the pore volume (g/cm) by applying the BET method. To remove eventual physisorbed species from the powder surface, the samples were outgassed at 250°C for 2 h prior to each analysis. The surface characteristics were determined from a nitrogen adsorption isotherm measured at 77 K with a conventional volumetric apparatus.

For the measurement of electrokinetic behavior of ceria suspension, the ceria particles were first dispersed in deionized water. A total of 220 ml of suspension for each powder was prepared at a weight fraction of 1%. Each suspension was subjected twice to ultrasonic treatment for 15 min in order to break down agglomerates and promote mixing. An ice bath was used to control the temperature of the suspension during the ultrasonic treatment. To establish an equilibrium dispersion system, the suspension was aged for 12 h at room temperature using a wrist-action shaker. Following aging, the suspension was ultrasonicated for an additional 15 min. The electrokinetic behavior of ceria suspensions was characterized using the electrokinetic sonic amplitude technique (ESA-9800, Matec Applied Sci., Hopkinton, MA, U.S.A.). In ESA tests, two identical suspensions were prepared for each analysis. Separate acid (1.0 N HCl) and base (1.0 N KOH) titrations were performed, beginning at the natural pH, and subsequently combined to generate a complete titration curve. Based on the analysis of preliminary measurement, the standard uncertainty yields ±0.1 $mPa \cdot m \cdot V^{-1}$ for ESA measurements and ±0.05 (pH units) for pH and IEP values, respectively. Details of this electroacoustic technique, its application to ceramic systems, and the estimated measurement precision, have been given in our previous papers.[20,21]

The CMP test was carried out using five different types of slurries with different calcination temperatures (400, 600, 700, 800, and 900°C). The ceria abrasives were dispersed in deionized water and stabilized by adding 100 ppm of a commercially available dispersant (Poly(methacylic acid), M.W. = 10000). We also added an anionic organic surfactant (Polyacrylic acid, M.W. = 50000) at weight fractions (based on solution content) of 0.5% in this experiment. Each slurry was diluted with deionized water to produce a final ceria abrasive concentration of 1 wt%. Each suspension pH was adjusted to the range of 7.0–8.0 by adding an alkaline agent. In CMP evaluation, a 200 mm wafer CMP tool (6EC, Strasbaugh, USA) was used. Oxide film was deposited by the plasma-enhanced tetra-ethyl-ortho-silicate (PETEOS) method. The thickness of the as-deposited oxide film was 7000 Å. A CMP tool for 200 mm wafers (6EC, Strasbaugh, USA) was used and *ex-situ* conditioning with a diamond dresser was carried out before CMP. The polishing pad was a grooved IC1000/Suba IV pad (Rodel, USA). The film thickness was measured with a Nanospec 180 (Nanometrics, USA) in order to determine the removal rate. After CMP, the wafers were cleaned with an APM solution ($NH_4OH : H_2O_2 : H_2O = 1 : 1 : 10$) at 80°C to eliminate residual particles. The polishing test conditions are listed in Table I.

Table I. CMP conditions.

Machine model	Strasbaugh 6EC
Slurry	Homemade slurry
Pad	IC1000/Suba IV k-groove
Table speed	70 rpm
Spindle speed	70 rpm
Down force	4 psi
Back pressure	0 psi
Time	30 s
Flow rate	100 ml/min

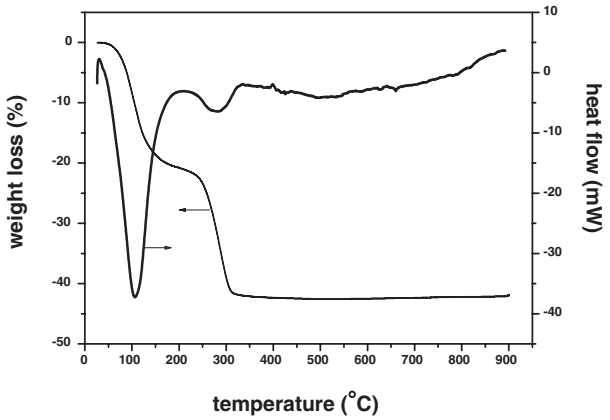

Fig. 1. Thermogravimetric and differential thermal analysis curves of the cerium carbonate precursor.

3. Results and Discussion

The thermal analysis results of the cerium carbonate precursor synthesized in this study are shown in Fig. 1. The total weight loss was approximately 40%. This result was indicative of the representative thermal decomposition behavior of the normal carbonates.[22] The decomposition of the cerium carbonate precursor had three distinct steps. The first step, mainly occurring at temperatures up to ~135°C, is due to the evaporation of the absorbed moisture and the release of molecular water. The second step, occurring in the range ~135–245°C, is due to the carbonate decomposition with oxycarbonate intermediates. Complete decomposition is almost achieved at 300–400°C, noting the oxidation of Ce^{3+} to Ce^{4+} during heating. The differential thermal analysis curve shows two exothermic peaks. As mentioned above, the first peak is due to the evaporation of the absorbed moisture and the release of molecular water. The second broad exotherm is due to the carbonate decomposition with the evolution of CO and CO_2, and assigned to crystallization. Similar results were found by other researchers.[22,23] Therefore, we can conclude that the carbonate was fully decomposed for all types of abrasive prepared in this study at a calcination temperature above 400°C.

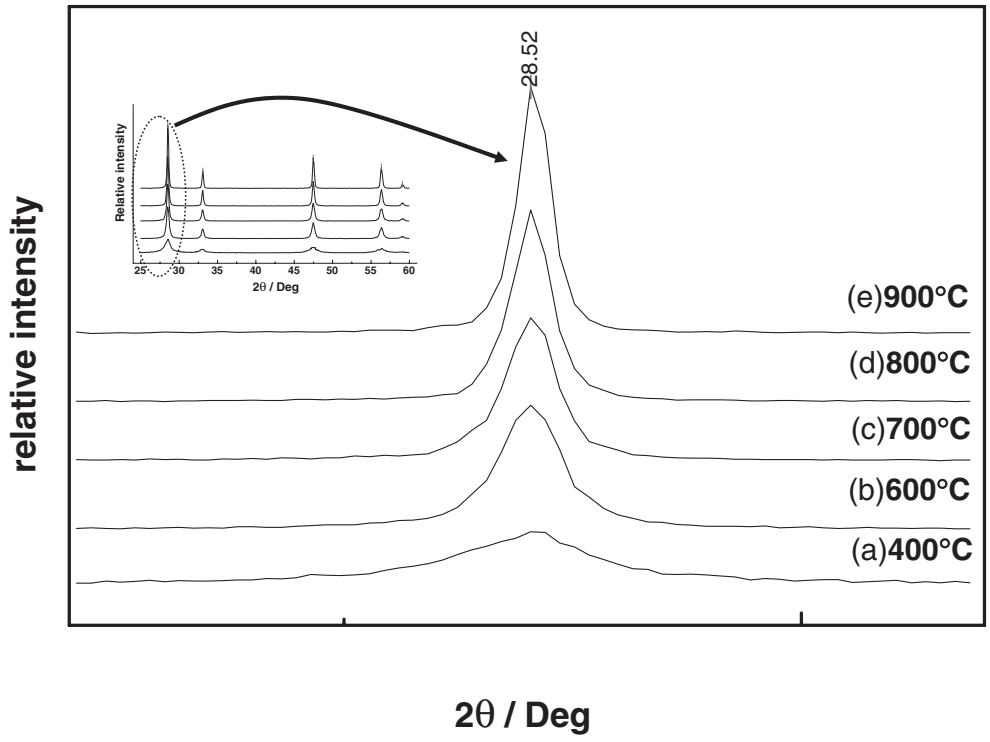

Fig. 2. X-ray powder diffraction patterns for ceria calcinated at various temperatures: (a) 400°C, (b) 600°C, (c) 700°C, (d) 800°C and (e) 900°C.

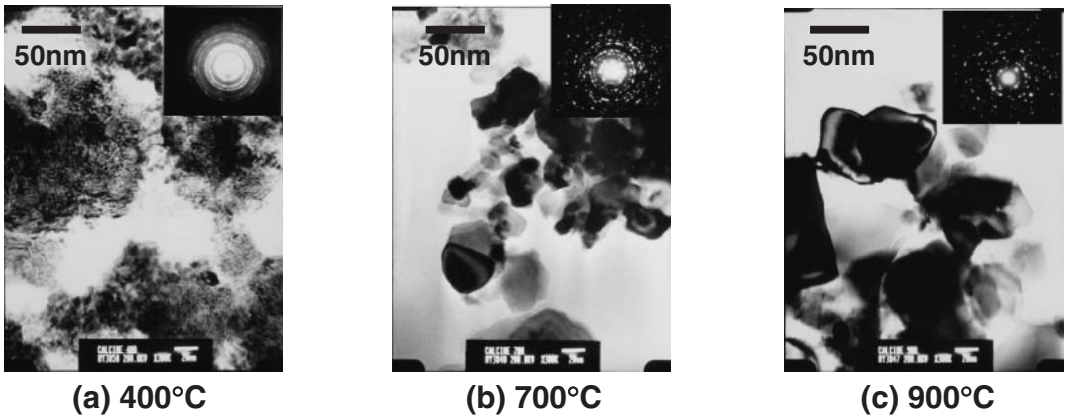

Fig. 3. TEM micrographs and diffraction patterns of particles calcined at various temperatures: (a) 400°C, (b) 700°C and (c) 900°C.

Figure 2 shows the X-ray diffraction (XRD) patterns of the powders calcined at different temperatures. Broad intensity peaks were observed for the ceria powders which were synthesized at 400°C. This result may be considered by the low crystallinity with unreacted carbonate. Although the oxidation of Ce^{3+} to Ce^{4+} at ~400°C is achieved, the grain size of cerium oxide, which was calcined at this temperature, was very small. This result is due to the small grains and unreacted carbonate, presented in the inner part of the cerium oxide. At the calcination temperature of 400°C, the oxidation of the cerium carbonate is not complete. Thus this cerium oxide is composed of cerium oxide on the surface and unreacted carbonate in the inner part of the particle. The diffraction pattern only shows the peaks of cerium oxide with a fluorite structure; those for other compounds, such as cerium carbonate and cerous oxide, were not detected. However, the cerium oxide, which was synthesized at 400°C, showed a broad intensity peak profile. With increasing calcination temperature, the characteristic peaks of CeO_2 became sharper,[24] because the grains of single crystals were proportionally grown by heat treatment. This result affected the average grain size of the particles. The grain size of CeO_2 was investigated to clarify the relationship between the calcination temperature and the physical characteristics of the particles. The line-broadening analysis of the (111) peak in XRD was analyzed to confirm the grain size of particles, as will be discussed later. We confirmed that CeO_2 abrasive with a good crystallinity was synthesized after calcination at 900°C.

Figure 3 shows the TEM images and diffraction patterns of the particles calcined at various temperatures (400, 700, and 900°C). These figures show that the grain size increased with calcination temperature, and that the morphology of the ceria particles varied according to the calcination temper-

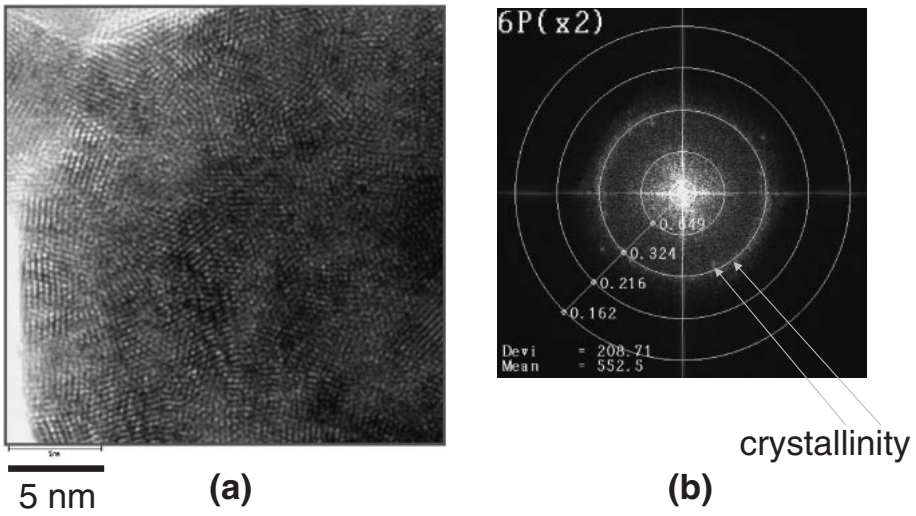

Fig. 4. HR-TEM image of particle calcined at 400°C: (a) lattice image, and (b) Fourier-transformed image.

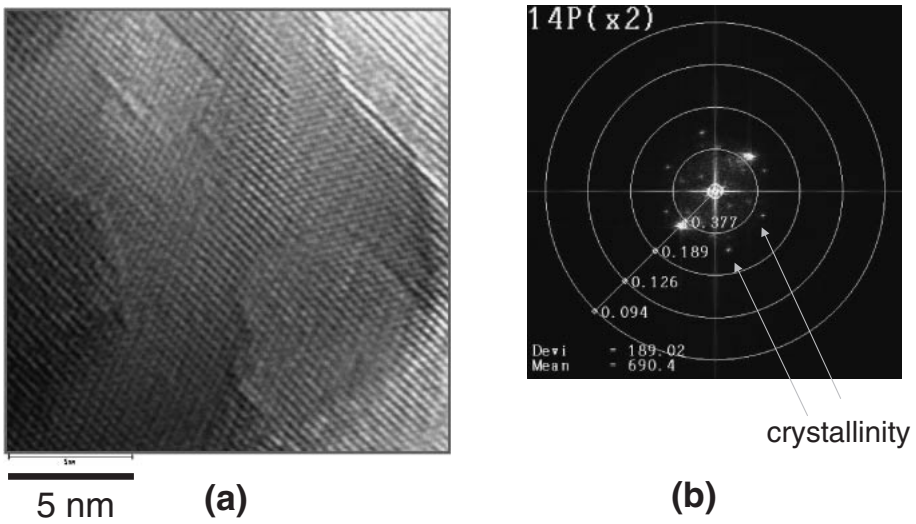

Fig. 5. HR-TEM image of particle calcined at 700°C: (a) lattice image, and (b) Fourier-transformed image.

ature. The particles calcined at 400°C [Fig. 3(a)] showed a relatively low crystallinity, whereas those calcined at 700°C [Fig. 3(b)] and 900°C [Fig. 3(c)] exhibited a relatively high crystallinity and the shapes of the grain are well-defined, though some grains seem to contain subgrain boundaries inside. The ring-shaped diffraction shown in Fig. 3(a) shows that the particles calcined at temperatures as low as 400°C still maintain their crystal structure. This result coincides with the XRD peaks shown in Fig. 2(a). The difference between the diffraction patterns of Figs. 3(b) and 2(c) is attributed to the number of grains in the objective aperture, or grain size. To investigate directly the atomic structure and crystallinity of the ceria particle in detail,[25] a high–resolution TEM (HR-TEM) image and its two-dimensional Fourier-transformed image were obtained. The lattice image of the ceria particle calcined at 400°C [Fig. 4(a)] clearly shows that the atomic structure of the particle has a rather long-range-ordering (LRO) at least longer than 5 nm. So we can conclude that it is not amorphous but fine polycrystalline. A number of dislocations and orientational domain structures are also shown. Figure 4(b) is the two-dimensional Fourier-transformed image of Fig. 4(a). The ring-like pattern shown in Fig. 4(b) corresponds to the fine polycrystalline structure with various orientations shown in Fig. 4(a). Figure 5 shows the lattice image of the ceria particle calcined at 700°C (a) and its Fourier-transformed image (b). The lattice image [Fig. 5(a)] shows the particle has a highly crystalline structure, though a few dislocations and stacking-faults were observed, which is also confirmed from Fig. 5(b). The results shown in Figs. 4 and 5 coincide well with those in Figs. 2 and 3.

The crystallinity of the ceria particles fabricated at various calcination temperatures was also studied. The grain sizes of the particles were estimated using the Debye–Scherrer equation[26] by utilizing XRD line broadening as

$$D = 0.9\lambda/(\beta\cos\theta),$$

where λ is the wavelength of the monochromatic X-ray beam, θ is the diffraction angle, and β is the half-width of an intensity peak. The intensity peak at $2\theta = 48^\circ$ was chosen for calculating the grain size, since it was clearer than any other peak and isolated from the others. As shown in Fig. 6,

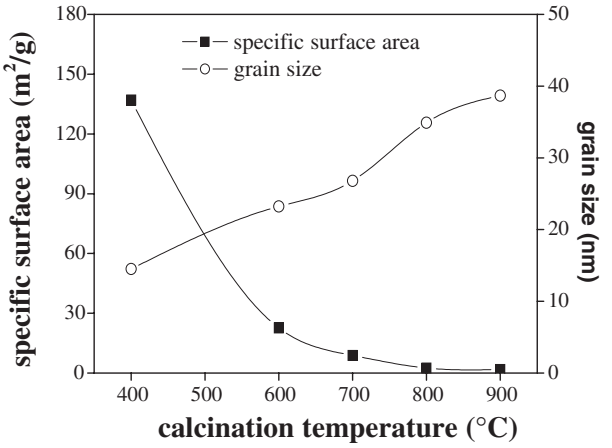

Fig. 6. Specific surface area (BET) and mean grain size (XRD) evolution as a function of calcination temperature.

Table II. Primary particle size of Ceria particle after calcination at various temperatures, as measured by TEM and calculated with the BET method.

		size (nm)
Calcination temperature (°C)	D_{TEM}	D_{BET}
400	5	3
600	—	18
700	35–40	47
800	—	166
900	80–90	229

the grain size moderately increased overall from 14.52 to 38.69 nm as the calcination temperature was increased from 400 to 900°C, and it rapidly increased from 700 to 800°C, which can be attributed to thermally promoted grain growth[27,28] during the calcination process. These results are in agreement with the trend of increasing grain size in the TEM images shown in Fig. 3.

The change in the specific surface area of the samples, measured by the BET method,[29] is also shown in Fig. 6. The particle calcined at 400°C had the highest surface area of 137 m^2/g. With increasing calcination temperature, the surface area continued to decrease and finally reached a value of 1.81 m^2/g at 900°C. The temperature dependence of the surface area is well correlated with the grain size, i.e., smaller grains have larger specific surface areas.[27] The particle size was calculated from the specific surface area by assuming that all powders were spherical without intra- or inter-pores, and that the densities of all the calcined powders were identical to that of pure cerium oxide (7.215 g/cm^3). The calculated values are listed in Table II. There was little difference between the calculated and measured grain sizes in the cases of the particles calcined at 400 and 700°C. On the other hand, there was a considerable difference between the two methods in the case of the particles calcined at 900°C, due to the occurrence of aggregation[25] of the particles at this temperature.

The total pore volume versus calcination temperature curve is shown in Fig. 7. Generally, pores exist in the particles as defects, which result from the decrease in the removal rate of PETEOS film. This is because such pores are

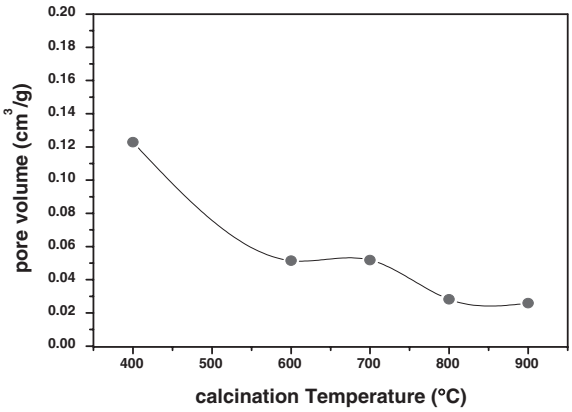

Fig. 7. Total pore volumes of particles calcined at various temperatures.

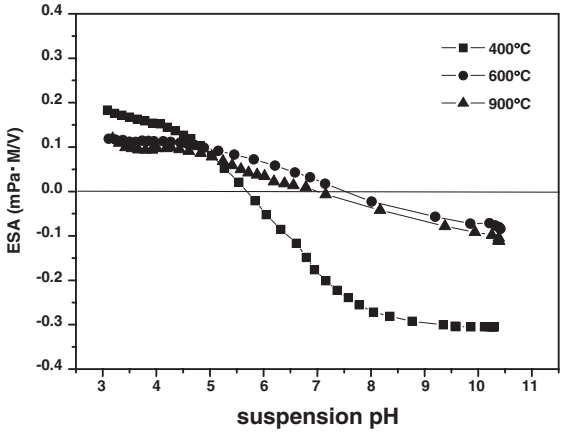

Fig. 8. Electrokinetic behaviors of particles calcined at various temperatures.

the cause of decreased particle density, resulting in the reduction of mechanical force between the abrasive and the film. The pore volume markedly decreased between the calcinations temperatures of 400°C and 600°C. As mentioned above, the particle calcined at 400°C is not a dense particle. Consequently many pores exist in the inner part of the particle. As the calcination temperature increases, the pore volume decreases with grain growth. The reduction in pore volume is saturated between the calcination temperatures of 800°C and 900°C.

The surface potential of the CeO_2 particles was measured as a function of pH by the ESA (electrokinetic sonic amplitude) technique. The electrokinetic behavior of the ceria suspensions is shown in Fig. 8. The electrophoretic mobility strongly depends on the suspension pH and the surface characteristics of the particle. Different electrokinetic behaviors were observed for the ceria powders calcined at 400°C. The isoelectric pH (pH_{iep}) of the particle calcined at 400°C is 5.5, but the pH_{iep} of CeO_2 particles calcined at 600 and 900°C is 7.5. This difference is due to the partial oxidation of the particle at the calcinations temperature of 400°C, resulting in different surface characteristics.

The results of the CMP field evaluation are shown in Fig. 9. As the calcination temperature increased, the ceria slurry for the STI CMP process had a higher removal rate for

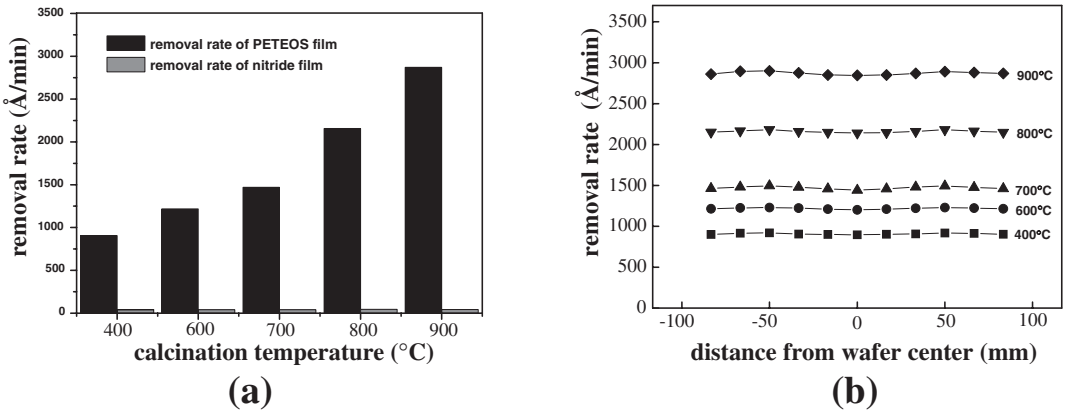

Fig. 9. Results of CMP field evaluation: (a) average PETEOS removal rate, and (b) within-wafer nonuniformity (WIWNU) of PETEOS.

the PETEOS film, rising from 907 Å/min at 400°C to 1471 Å/min at 700°C. Above 700°C, the PETEOS removal rate rapidly increased to 2871 Å/min at 900°C. On the other hand, the removal rate for CVD Si_3N_4 film remainde at 40 Å/min at 400°C and 49 Å/min at 900°C, and did not vary much with calcinations temperature. Thus the oxide-to-nitride selectivity increases with calcination temperature, from 23 at 400°C to 59 at 900°C. The polishing of PETEOS is mainly affected by its chemical interaction with the CeO_2 particles, and by physical factors, including the physical properties of the particles, the mechanical grinding factor, and so forth.

The surface of PETEOS film is soluble in alkaline pH solutions due to the dissolution of Si ions. Interaction between the film surface and the ceria particles occurs during the polishing of the PETEOS film, and Si–O–Ce bonds are then formed on the film surface. The Si–O–Ce bonding has been reported to be the dominant mechanism in the chemical interaction between PETEOS film and ceria particles.[4] The pH was maintained constant for all slurries in this experiment; thus, it can be asserted that the increase in the removal rate of PETEOS with the calcination temperature is related to the physical factors rather than to the chemical interaction. These physical factors are impacted by several aspects of the STI CMP process, such as the CMP conditions, abrasive particle morphology, particle size and distribution, and grain size. As seen from Fig. 3, the abrasive particles calcined at 400°C had different morphologies as compared with the other particles. The removal rate can be significantly affected by mean particle size and agglomerated particle size, because frictional force is directly proportional to contact area.[30] The morphology of the particles calcined at 400°C and the slight increase in particle size above a calcination temperature of 700°C cannot account for the continued increase in removal rate with calcination temperature. Instead, as shown in Fig. 6, the grain size increased with calcination temperature, which resulted in the increase in the removal rate of PETEOS film. On the other hand, the surface of the Si_3N_4 film during polishing is thought to be passivated with adsorptive surfactant in the slurry, which prevents the abrasive from directly contacting the film surface.[8,31,32] Hence, the removal rates for Si_3N_4 film did not vary much regardless of grain size increasing with calcination temperature.

4. Conclusions

We prepared abrasive ceria particles by controlling the calcination temperature (in the solid-state decomposition method) and conducted a CMP evaluation using these particles. We investigated the effect of increasing calcination temperature on the physical properties of the particles. The relationship between the physical properties of ceria particles and the removal rate of PETEOS film was thus identified. As calcination temperature increased, the crystallization degree of the particles increased and the ceria slurry for the STI CMP process had a higher removal rate for PETEOS film. It can be concluded that the grain size is the key factor accounting for the increase in the PETEOS removal rate with the calcination temperature.

Acknowledgements

This work was financially supported by the Korea Institute of Science and Technology Evaluation and Planning (KISTEP) through the National Research Laboratory (NRL) Program. We thank Dr. Alexander Tikhonovsky for helping us with our HR-TEM analysis.

1) S.-H. Lee, Z. Lu, S. V. Babu and E. Matijevic: J. Mater. Res. **17** (2002) 2744.
2) S. K. Kim, S. K. Lee, U. Paik, T. Katoh and J. G. Park: J. Mater. Res. **18** (2003) 2163.
3) T. Katoh, S. J. Kim, U. Paik and J. G. Park: Jpn. J. Appl. Phys. **42** (2003) 5430.
4) L. M. Cook: J. Non-Cryst. Solids **120** (1990) 152.
5) J. Y. Kim, S. K. Kim, U. Paik, T. Katoh and J. G. Park: J. Korean Phys. Soc. **41** (2002) 413.
6) H. Park, K. B. Kim, C. K. Hong, U. I. Chung and M. Y. Lee: Jpn. J. Appl. Phys. **37** (1998) 5849.
7) T. Hoshino, Y. Kurata, Y. Terasaki and K. Susa: J. Non-Cryst. Solids **283** (2001) 129.
8) J. G. Park, T. Katoh, W. M. Lee, H. Jeon and U. Paik: Jpn. J. Appl. Phys. **42** (2003) 5420.
9) S. K. Kim, U. Paik, S. G. Oh, Y. K. Park, T. Katoh and J. G. Park: Jpn. J. Appl. Phys. **42** (2003) 1227.
10) G. A. M. Hussein: J. Anal. Appl. Pyrolysis **37** (1996) 111.
11) B. Djuricic and S. Pickering: J. Eur. Ceram. Soc. **19** (1999) 1925.
12) J. L. G Fierro, S. Mendioroz and A. M. Olivan: J. Colloid Interface Sci. **100** (1984) 303.
13) F. Czerwinsky and J. A. Szpunar: Proc. Mater. Res. Soc. Symp. **343** (1994) 535.
14) M. Hirano and E. Kato: J. Am. Ceram. Soc. **82** (1999) 786.

15) Y. Zhou, R. J. Phillips and J. A. Switzer: J. Am. Ceram. Soc. **78** (1995) 981.
16) H. Hahn, J. A. Eastman and R. W. Siegel: Ceram. Trans. 1b, Ceram. Powder Sci. (1988) 1115.
17) T. Tsuzuki and P. G. McCormick: J. Am. Ceram. Soc. **84** (2001) 1453.
18) F. Bondioli, A. Bonamartini Corradi, C. Leonelli and T. Manfredini: Mater. Res. Bull. **34** (1999) 2159.
19) P. Klug and L. E. Alexander: *Diffraction Procedures for Polycrystalline and Amorphous Materials* (John Wiley & Sons, New York, 1954) Chap. 9.
20) V. A. Hackley and U. Paik: *Ultrasonic and Dielectric Characterization Techniques for Suspended Particulates*, ed. V. A. Hackley and J. Texter (J. Am. Ceram., Westerville, 1998) p. 191.
21) V. A. Hackley, U. Paik, B. Kim and S. Malghan: J. Am. Ceram. Soc. **80** (1997) 1782.
22) E. L. Head and C. E. Holly, Jr.: *Rare Earth Research II*, ed. K. S. Vorres (Gordon and Breach, London, 1964) p. 51.
23) Y. Wang, T. Mori, J.-G. Li, T. Ikegami and Y. Yajima: J. Mater. Res. **18** (2003) 1239.
24) P.-L. Chen and I.-W. Chen: J. Am. Ceram. Soc. **76** (1993) 1577.
25) D. Terribile, A. Trovarelli, J. Llorca, C. de Litenburg and G. Dolcetti: J. Catal. **178** (1998) 299.
26) Y. X. Li, X. Z. Zhou, Y. Wang and X. Z. You: Mater. Lett. **58** (2003) 245.
27) X. Yu, F. Li, X. Ye and X. Xin: J. Am. Ceram. Soc. **83** (2000) 964.
28) M. Hirano and E. Kato: J. Mater. Sci. Lett. **18** (1999) 403.
29) T. Tsuzuki and P. G. McCormick: J. Am. Ceram. Soc. **84** (2001) 1453.
30) U. Mahajan, M. Belmann and R. K. Singh: Electrochem. Solid-State Lett. **2** (1999) 46.
31) K. Hirai, H. Ohtsuki, T. Ashizawa and Y. Kurata: Hitachi Chemical Tech. Report No. 35 (2000) p. 17.
32) Y. Homma, T. Furusawa, H. Morishima and H. Sato: Solid-State Electron. **41** (1997) 1005.